Properties of Ion-Implanted High-Power Angled-Grating Distributed-Feedback Lasers

Katrin Paschke, Alexander Bogatov, Frank Bugge, Alexander E. Drakin, Jörg Fricke, Reiner Güther, Alexey A. Stratonnikov, Hans Wenzel, Götz Erbert, *Member, IEEE,* and Günther Tränkle, *Member, IEEE*

***Abstract*—An improvement of the linearity of the light–current characteristics and the beam quality of high-power α-distributed feedback lasers is achieved by an ion implantation of the regions outside the contact stripe. The linear part of the light–current characteristics of 4-mm-long devices emitting at 1060 nm is extended to $P = 1.8$ W output power. The times-diffraction-limit factor M^2 remains constant, equal to 1.7 over the whole power range. Simulations of the electro-optical behavior reveal that the improvement is achieved by a suppression of optical field components which propagate inside the cavity perpendicular to the facets.**

***Index Terms*—Angled grating, distributed feedback (DFB) laser, high-power semiconductor laser, implantation, simulation, slanted Bragg grating.**

I. Introduction

SUBSTANTIAL effort has been devoted to the development of semiconductor lasers which emit simultaneously a nearly diffraction-limited beam and a high optical power. Besides hybrid master-oscillator power-amplifier (MOPA) configurations, there are a few monolithic laser types with more than 1 W diffraction-limited output power. Among them are the monolithically integrated flared amplifier (MFA) MOPA with 2 W maximum continuous-wave (cw) output power [1], the tapered laser with a maximum cw output power in the range of 3–4 W [2], [3], and the angled-grating distributed-feedback (α-DFB) laser emitting up to 3 W [4]–[9]. Common for both the tapered laser and the α-DFB laser are special filtering mechanisms in order to suppress higher order modes.

In a tapered laser, one section of the cavity consists of a fundamental lateral-mode waveguide [e.g., a ridge waveguide (RW)]. Higher order modes excited in the tapered section are not able to propagate in the RW and are thus damped away. A disadvantage of tapered lasers is the big astigmatism of the emitted beam and the non-Gaussian shape of the true far field. In an α-DFB laser, there is a Bragg grating integrated into the whole cavity. Whereas in conventional DFB lasers, the grooves are directed parallel to the facets, here the grooves, as well as the contact stripe (CS), are slightly slanted with respect to the cavity axis perpendicular to the facets. The mode filtering is achieved by distributed diffraction at the slanted Bragg grating [4]–[7] and can be related to the angular and wavelength selectivity of volume hologram gratings [10]. This distributed diffraction leads to a beating between two waves with a periodical exchange of energy.

Manuscript received February 14, 2003; revised August 27, 2003. This work was supported by the Deutsche Forschungsgemeinschaft under Contract SE 954/1-2.

K. Paschke, F. Bugge, R. Güther, J. Fricke, H. Wenzel, G. Erbert, and G. Tränkle are with the Ferdinand-Braun-Institut für Höchstfrequenztechnik, 12489 Berlin, Germany (e-mail: paschke@fbh-berlin.de).

A. Bogatov, A. Drakin, and A. Stratonnikov are with the P. N. Lebedev Physical Institute, 119991 Moscow, Russia.

Digital Object Identifier 10.1109/JSTQE.2003.820915

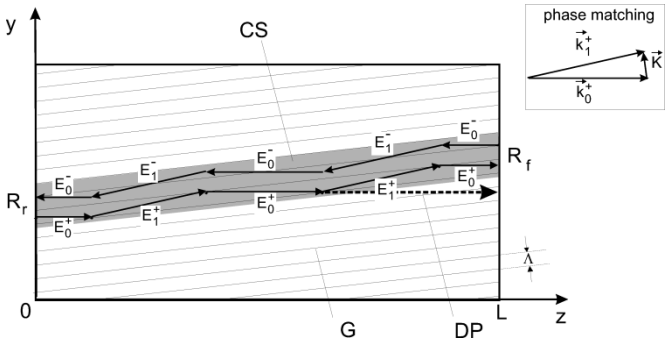

Fig. 1. Schematic top view of an α-DFB laser in the yz plane (CS: contact stripe, G: Bragg grating, DP: direct path, Λ: grating period, L: cavity length, R_r: reflectivity of rear facet, R_f: reflectivity of front output facet, E_0^+ and E_1^+: forward propagating coupled wave pair, and E_0^- and E_1^-: backward propagating coupled wave pair).

The power loss from this pair of coupled waves by sideward emission has to be minimized by a proper design. A second loss mechanism is the limited effectiveness of the Bragg grating, since the reflection from the facets favors propagation perpendicular to the facets as part of the radiation travels along a "direct path" to the facets, as denoted in Fig. 1 by DP. Especially at a higher output power, this "direct path" disturbs the light–current characteristic and leads to unwanted side lobes in the near and far fields, which enhance the times-diffraction-limit factor M^2.

In order to suppress the direct path, the introduction of highly absorbing regions near the facet was proposed in [11] and [12]. Here, we present a similar effect by an implantation of the regions outside the contact stripe.

The paper is organized as follows. In Section II, a short description of our numerical model for α-DFB lasers is given and the impact of an implantation on the field distributions within the cavity is shown. In Section III, some details of the fabrication process are presented, and in Section IV, theoretical and experimental light current as well as beam characteristics of nonimplanted and implanted devices are compared. Finally, in Section V, the main conclusions are drawn.

II. Theoretical Model

A schematic top view of an α-DFB laser is shown in Fig. 1. The laser chip with length L is bounded by the rear facet having a high reflectivity R_r and by the front output facet having a low

reflectivity R_f. The angled Bragg grating G is described by the Bragg grating vector

$$\mathbf{K} = \frac{2\pi}{\Lambda}(0, \cos\alpha_G, -\sin\alpha_G) \tag{1}$$

where Λ is the period of the grating and α_G the slant angle. The CS with width w runs parallel to the grating grooves.

In Fig. 1, the propagation direction of the forward- and backward-propagating coupled waves $E_0^{\pm}$ and $E_1^{\pm}$ are sketched, too. Their treatment follows the standard procedure of the coupled wave theory of volume holograms proposed by Kogelnik [10]. The wave E_0^+ with wave vector

$$\mathbf{k}_0 = \left(0, 0, \frac{n_{\text{eff}}\omega}{c}\right) \tag{2}$$

corresponds to the reconstruction wave, and the wave E_1^+ with wave vector $\mathbf{k}_1 = \mathbf{k}_0 + \mathbf{K}$ (compare Fig. 1) to the reconstructed signal wave in [10] and similar to the direction-inverted waves. The Bragg condition for a first-order grating reads

$$K = 2n_{\text{eff}}\frac{\omega}{c}\sin\alpha_G \tag{3}$$

with n_{eff} the effective index of the vertical waveguide, ω the circular frequency, and c the velocity of light. Equation (3) leads to the fact that $|\mathbf{k}_0| = |\mathbf{k}_1|$ holds for this ω and this α_G. In the following, we present the basic procedure to solve the Helmholtz equation and the final equations to be fulfilled by $E_0^{\pm}$ and $E_1^{\pm}$.

The Helmholtz equation with a periodic variation of the dielectric function reads

$$\Delta\mathbf{E} + \frac{\omega^2}{c^2}\left[n_{\text{eff}}^2 + 2n_{\text{eff}}\Delta n_G\cos(\mathbf{Kr}) + \varepsilon_M\right]\mathbf{E} = 0 \tag{4}$$

with $\mathbf{E}$ the electric field vector, $\mathbf{r} = (0, y, z)$ the position vector, Δn_G the amplitude of the first Fourier component of the refractive index Bragg grating, and ε_M containing additional contributions to the dielectric constant to be discussed later on [see (12)]. The relation between Δn_G and the often-used coupling constant κ [10] reads

$$\Delta n_G = \frac{2\kappa c}{\omega}. \tag{5}$$

After the electric field is decomposed into the two pairs of forward and backward traveling waves [10]

$$\begin{aligned}\mathbf{E} = \frac{1}{2}\big[&\mathbf{e}_0 E_0^+(y,z)\mathrm{e}^{ik_0 z} + \mathbf{e}_1 E_1^+(y,z)\mathrm{e}^{i\mathbf{k}_1\mathbf{r}} \\ &+\mathbf{e}_0 E_0^-(y,z)\mathrm{e}^{-ik_0 z} + \mathbf{e}_1 E_1^-(y,z)\mathrm{e}^{-i\mathbf{k}_1\mathbf{r}}\big]\,\mathrm{e}^{-i\omega t} + \text{c.c.}\end{aligned} \tag{6}$$

with the slowly varying amplitudes E_0^+, E_1^+, E_0^-, and E_1^-, the unit vectors $\mathbf{e}_0 = (0,1,0)$, $\mathbf{e}_1 = (0, \cos(2\alpha_G), -\sin(2\alpha_G))$, and $c.c$ denoting the complex conjugate. The substitution of (6) in (4), the consideration of terms of zeroth and first diffraction order only, and the neglect of the second-order derivative with respect to z lead to two times two coupled wave equations

$$\begin{aligned}\frac{\partial}{\partial z}E_0^+ = \frac{i}{2k_0}\left\{\left[\frac{\omega^2}{c^2}\varepsilon_M + \frac{\partial^2}{\partial y^2}\right]E_0^+\right. \\ \left.+n_{\text{eff}}\Delta n_G\cos(2\alpha_G)\frac{\omega^2}{c^2}E_1^+\right\}\end{aligned} \tag{7}$$

$$\begin{aligned}\frac{\partial}{\partial z}E_1^+ = \frac{i}{2k_{1z}}\left\{\left[\frac{\omega^2}{c^2}\varepsilon_M + \frac{\partial^2}{\partial y^2} + 2ik_{1y}\frac{\partial}{\partial y}\right]E_1^+\right. \\ \left.+n_{\text{eff}}\Delta n_G\cos(2\alpha_G)\frac{\omega^2}{c^2}E_0^+\right\}\end{aligned} \tag{8}$$

$$\begin{aligned}\frac{\partial}{\partial z}E_0^- = \frac{i}{2k_0}\left\{\left[\frac{\omega^2}{c^2}\varepsilon_M + \frac{\partial^2}{\partial y^2}\right]E_0^-\right. \\ \left.+n_{\text{eff}}\Delta n_G\cos(2\alpha_G)\frac{\omega^2}{c^2}E_1^-\right\}\end{aligned} \tag{9}$$

$$\begin{aligned}\frac{\partial}{\partial z}E_1^- = \frac{i}{2k_{1z}}\left\{\left[\frac{\omega^2}{c^2}\varepsilon_M + \frac{\partial^2}{\partial y^2} - 2ik_{1y}\frac{\partial}{\partial y}\right]E_1^-\right. \\ \left.+n_{\text{eff}}\Delta n_G\cos(2\alpha_G)\frac{\omega^2}{c^2}E_0^-\right\}\end{aligned} \tag{10}$$

with $\cos(2\alpha_G) = \mathbf{e}_0 \cdot \mathbf{e}_1$. The inclusion of the $\cos(2\alpha_G)$ factor results from the transverse electric (TE)-like polarization of the waves, where this polarization is defined by the polarization vectors $\mathbf{e}_0$ and $\mathbf{e}_1$ lying in the yz plane (compare [10, eq. (90)]).

At the facets, the field amplitudes have to fulfill the boundary conditions

$$\begin{aligned}E_0^+(y,0) &= R_r^{\frac{1}{2}}E_0^-(y,0) \\ E_1^+(y,0) &= 0 \\ E_0^-(y,L) &= R_f^{\frac{1}{2}}E_0^+(y,L) \\ E_1^-(y,L) &= 0.\end{aligned} \tag{11}$$

These conditions can be motivated as follows. The wave E_0^- is the direction-inverted wave of E_0^+. E_0^- and E_0^+ propagate perpendicular to the facets and fulfill the usual reflecting boundary conditions. It is worth mentioning that via these boundary conditions, the two groups of coupled wave equations (7), (8) and (9), (10) are linked. Similarly, E_1^+ is the direction-inverted wave to E_1^-. However, at the facets E_1^+ is not generated by E_1^-, because the direction of the reflected wave of E_1^+ is unequal to the direction of the wave E_1^-, and vice versa. The reflected waves of E_1^- and E_1^+ propagate toward the absorbing regions outside the CS and possibly leave the chip at the side walls [13]. Because they are reflected under the angle of total reflection, they do not contribute to the transmitted power, too. Hence, the output power at the output facet is given by $P \propto \int_{-\infty}^{+\infty}|E_0^+(y,L)|^2 dy$. The boundary conditions for $y \to \pm\infty$, namely, the existence of outgoing waves only, are modeled by the introduction of barrier regions with randomly fluctuating index and absorption.

Equations (7)–(10) are solved with a Fox–Li-like roundtrip algorithm. It is started at the rear facet with a guess distribution for $E_0^{+(0)}(y,0)$ and with $E_1^{+(0)}(y,0) = 0$, which are propagated to the front facet using (7) and (8). Then the boundary conditions (11) are applied, and the fields are propagated back to the rear facet using (9) and (10), where again the boundary conditions (11) are applied, and so on, until $E_0^{+(n)}(y,0)$ converges after n roundtrips. Numerically, each of (7)–(10) is split into two parts and the solution is performed employing a split-step algorithm [14], [15].

Now, the additional contributions to the dielectric function to be contained in ε_M in (4) are shortly discussed. Details can be found in [8]. It consists of four terms

$$\varepsilon_M = \varepsilon_B + \varepsilon_T + i\frac{c}{\omega} n_{\text{eff}} \alpha_n + \varepsilon_N. \tag{12}$$

Here, ε_B describes the dependence of ε on the index and absorption fluctuations in the barrier regions in order to model the boundary conditions for $y \to \pm\infty$, and ε_T is the change of ε caused by self-heating. The corresponding temperature profile is obtained from a solution of the one-dimensional heat conduction equation using the Greens function method. The absorption coefficient α_n determines the supplementary losses. ε_N describes the carrier influence on ε

$$\varepsilon_N = 2n_a \frac{\partial n}{\partial N} N\Gamma - i\frac{c}{\omega} n_a g(N)\Gamma \tag{13}$$

with n_a the active region refractive index, Γ the active region optical confinement factor, and N the carrier concentration. The change of the refractive index with carrier concentration is given by the parameter $\partial n/\partial N$ and the material gain is defined as

$$g(N) = \begin{cases} g_0 \ln\left[\frac{N}{(b+cN)}\right], & N > N_{\text{cr}} \\ g_0\left[\frac{1}{2}\left(\frac{N}{N_{\text{cr}}}\right)^2 - 1\right], & 0 \le N < N_{\text{cr}} \end{cases} \tag{14}$$

where $g_0, b,$ and c are parameters fitted on a theoretical gain model [8]. $N_{\text{cr}} = b(\mathrm{e}^{1/2} - c)^{-1}$ is determined such that (14) is a continuous function (values of gain parameters: $g_0 = 1892.2\ \text{cm}^{-1}$, $b = 0.96\ \text{cm}^{-1}$, $c = 0.0925\ \text{cm}^{-1}$, and $N_{\text{cr}} = 0.62\ \text{cm}^{-1}$).

The profile of the carrier density is obtained by solving a one-dimensional diffusion equation, taking into account the stimulated recombination.

For a given current through the CS in Fig. 1, the Fox–Li algorithm yields the distributions of the electromagnetic field and the carrier density. At the output facet, the emitted near-field profile can be calculated, and from this, the far-field profile by Fourier transformation and the light–current characteristics. More details of the calculation are given in [8].

Fig. 2 shows the obtained intensity distribution $|E_0^+(y,z)|^2$ of an α-DFB laser with slant angle $\alpha_G = 15°$, stripe width $w = 160\ \mu$m, cavity length $L = 4$ mm, $\Delta n_G = 0.004\,36$, rear facet reflectivity $R_r = 94\%$, front facet reflectivity $R_f = 0.1\%$, output power $P = 0.8$ W, and heat sink temperature $T_s = 25°$C. E_0^+ is the most interesting wave of the four waves E_0^+, E_1^+, E_0^-, E_1^-, because it is transmitted at the front facet to constitute the near field. The coupling of the wave pair E_0^+ and E_1^+ results in a chain of maxima of the intensity distribution $|E_0^+(y,z)|^2$. The right part of Fig. 2(b) shows details of the left part (a). The intensity distribution of $|E_0^+(y,z)|^2$ shows a "finger-shaped" structure which points almost perpendicular to the facets and appears as a side lobe in the near field, especially at higher output power.

Mainly, the influence of the implantation outside the CS was modeled by a large loss $\alpha_n = 50\ \text{cm}^{-1}$, whereas the loss is within the stripe $\alpha_n = 1\ \text{cm}^{-1}$. An additional modification of the refractive index in the implanted range will be discussed in Section IV. The result of modeling is shown in Fig. 3. The finger structure disappeared, i.e., the side lobe in the near field should be suppressed. Due to this theoretical finding, an experimental realization seemed to be very promising.

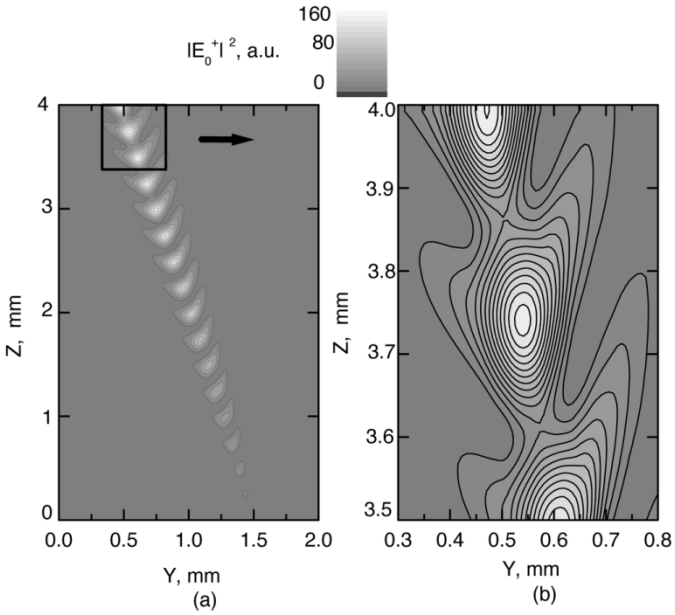

Fig. 2. Grey-scale plot of $|E_0^+(y,z)|^2$ for an α-DFB laser with $\alpha_G = 15°$, $w = 160\ \mu$m, $\Delta n_G = 0.004\,36$, $R_r = 94\%$, $R_f = 0.1\%$, and $L = 4000\ \mu$m at $P = 0.8$ W. (a) Whole chip area. (b) Magnification of (a) near the output facet.

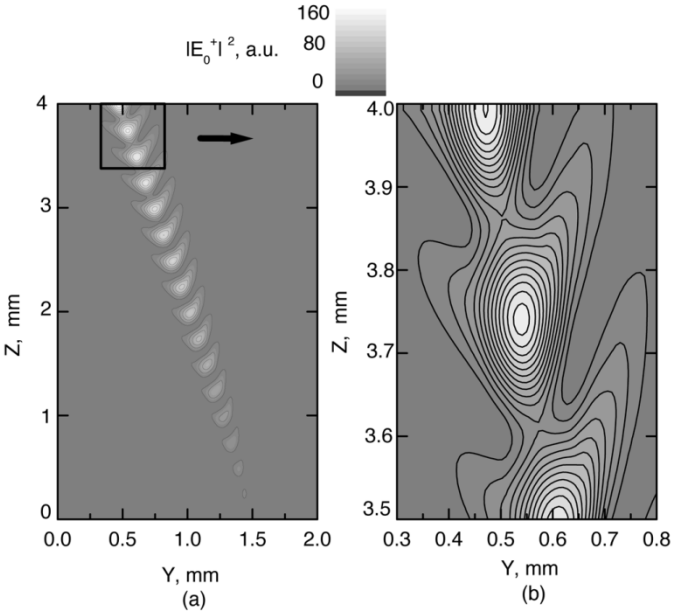

Fig. 3. Grey-scale plot of $|E_0^+(y,z)|^2$ for an ion-implanted α-DFB laser with the same parameters as in Fig. 2. (a) Whole chip area. (b) Magnification of (a) near the output facet.

III. Fabrication of α-DFB Lasers

A schematic view of an α-DFB laser is shown in Fig. 4. The layer structure was grown by a two-step metal-organic vapor-phase epitaxy (MOVPE). During the first step, the n-doped $Al_{0.25}Ga_{0.75}As$ cladding, the 400-nm thick n-doped GaAs waveguide, the undoped InGaAs quantum well (QW) with emission wavelength of about 1.06 μm, and the 400-nm

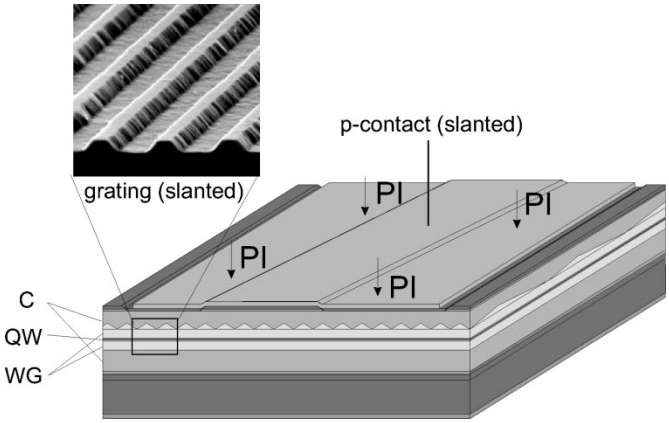

Fig. 4. Schematic view of an α-DFB laser (QW: quantum well; WG: waveguide; C: cladding layer; PI: proton implantation).

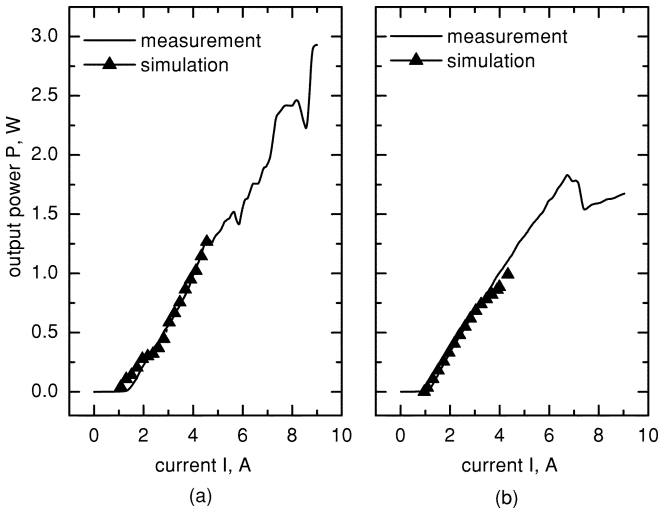

Fig. 5. Theoretical (triangles) and experimental (solid line) light–current characteristics of: (a) a nonimplanted, and (b) an implanted α-DFB laser with $\alpha_G = 15°$, $w = 160$ μm, $R_r = 94\%$, $R_f = 0.1\%$, and $L = 4$ mm. The heat sink temperature is $T_S = 25°$C. In the simulation, $\Delta n_G = 0.004\,36$ was assumed.

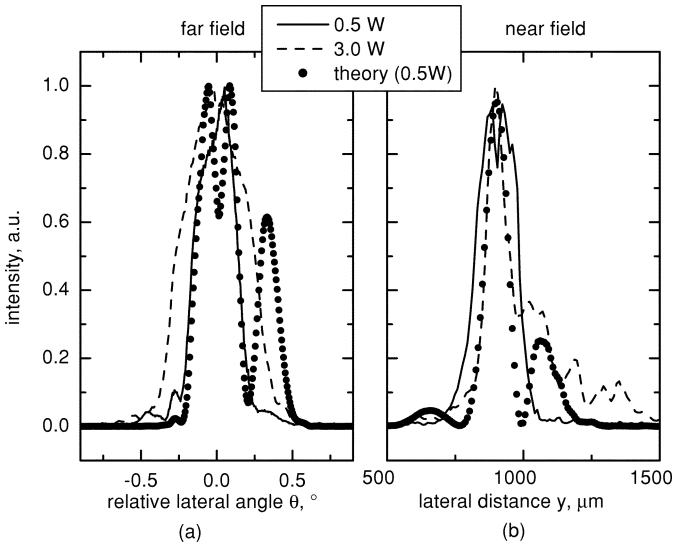

Fig. 6. Theoretical (bullets) and experimental (lines) intensity profiles of (a) near field and (b) far field of the nonimplanted device of Fig. 5 for different output power.

thick p-doped GaAs waveguide were grown. Then, the slanted Bragg grating was formed on top of the waveguide by stepper lithography and wet-chemical etching.

From scanning electron microscopy (SEM) pictures, the etch depth of the grating was determined to range between 120–150 nm and the duty cycle between 0.3 and 0.4. From a solution of the vertical waveguide equation values of Δn_G, between 0.0035–0.006 were obtained. The grating period is $\Lambda = 594$ nm for an intended emission wavelength of $\lambda = 1.06$ μm in accordance with the Bragg condition (3).

After cleaning the surface, the p-doped $Al_{0.25}Ga_{0.75}As$ cladding and the p-doped GaAs contact layer were grown in the second step. Finally, the slanted p-CS is defined by removal of the contact layer outside the stripe and opening of the insulation. The regions outside of the CSs of some devices were additionally implanted with H^+ ions (protons) with a kinetic energy of 250 keV and a dose of 10^{15} cm^{-2} up to the QW. For the measurements of the radiative characteristics, the lasers were soldered p-side down on CuW subcarriers and bonded on copper heatsinks. Further details of the structure and fabrication process were described in [16].

IV. Experimental Results and Comparison With Simulation

In this section, we compare nonimplanted and implanted α-DFB lasers with a slant angle of $\alpha_G = 15°$, a contact width of $w = 160$ μm, a cavity length of $L = 4$ mm, and facet reflectivities of $R_r = 94\%$ and $R_f = 0.1\%$. The measurements were performed under quasi-CW-conditions with a pulse length of 1 ms (repetition 25 Hz) at room temperature ($T_S = 25°$C).

In Fig. 5, measured (solid lines) and simulated (symbols) light–current characteristics of nonimplanted and implanted devices are compared. A maximum output power of 3 W limited by the electrical current supply was achieved for nonimplanted devices. However, above $P = 1.3$ W, the characteristic becomes rather kinky. For the implanted device, the characteristic remains almost linear up to 1.8 W. The decrease of the maximum output power to 1.8 W for the implanted device is not clear yet. Possibly, by a variation of device or implantation parameters, the maximum output power could be increased again. This is currently under study. It should be noted that the efficiency of the implanted device is slightly smaller compared to the nonimplanted one.

In the simulations, the exact value of the index modulation Δn_G has been treated as a fitting parameter in the range given above. The agreement of the simulated light–current characteristics with the experimental ones is quite good until the occurrence of numerical instabilities in the algorithm at an current of about $I = 4.5$ A.

Figs. 6 and 7 show the theoretical (bullets) and experimental (lines) far-field and near-field intensity profiles of the nonimplanted respective implanted devices. The side lobes visible in the theoretical and experimental intensity profiles of the nonimplanted device disappeared for the implanted device. Thus, the ion implantation of the regions outside the CS yielded exactly

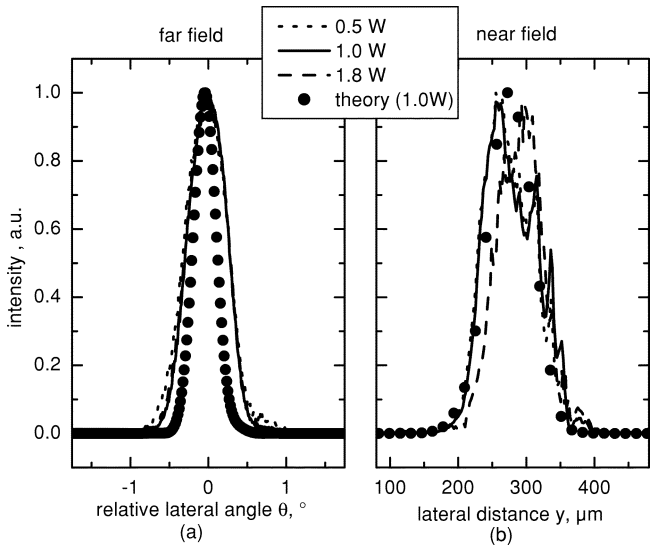

Fig. 7. Theoretical (circles) and experimental (lines) lateral far and near field intensities with implantation for the same device as in Fig. 5(b). (a) Far field. (b) Near field for different output power.

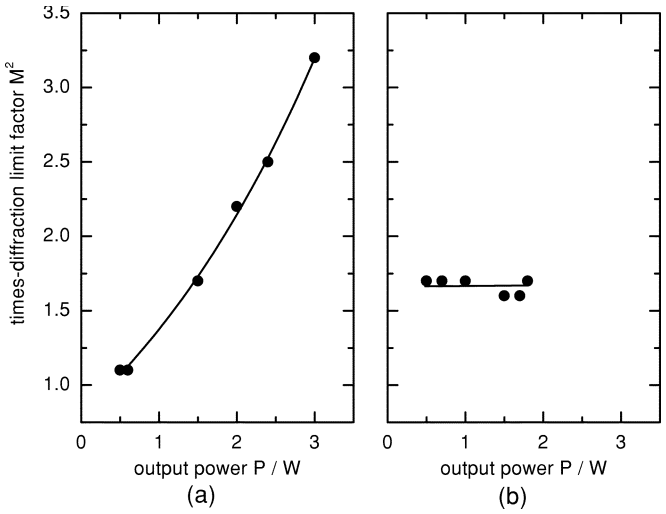

Fig. 8. Measured times-diffraction-limit factor for the devices of Figs. 5 versus output power. (a) No implantation. (b) With implantation.

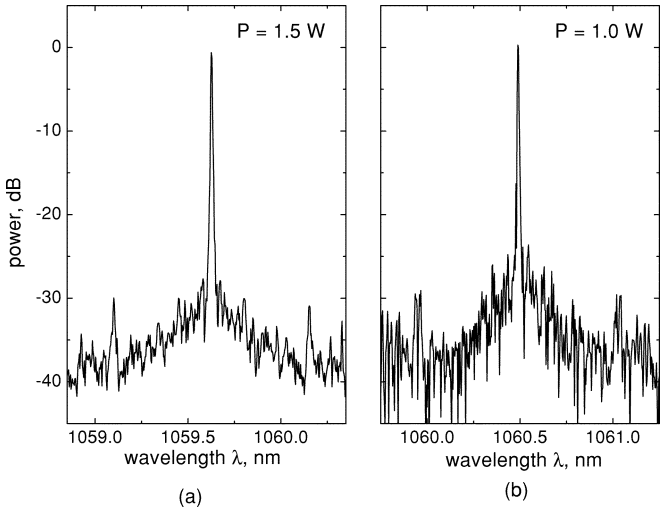

Fig. 9. Optical spectrum of the device of Fig. 5 measured at 1.5 and 1.0 W. (a) No implantation. (b) With implantation.

the result predicted by the simulations (compare Figs. 2 and 3, too).

The implantation acts in different ways. First of all, the conductivity of the affected layers is decreased by a factor of 10^{-3} and smaller. This leads to a strongly reduced current spreading effect. Secondly, because the QW outside the CS region was implanted, too, the Shockley–Read–Hall carrier lifetimes (recombination via deep centers) there are strongly diminished. Both effects cause a narrowing of the lateral profile of the excess carrier density in the QW, and even more narrowing of the gain profile. But the inclusion of these effects did not explain the measured shape of the near-field intensity. As a third effect, the decrease of the refractive index by implantation was included with the result of a decisive narrowing of the near field. Within the stripe, the refractive index is $n_a = 3.6$ and the loss $\alpha_n = 1\ \mathrm{cm}^{-1}$. The best fit of the measured near-field intensity with the calculated near field yielded the values of the complex index in the implanted range with the index $n_{\mathrm{implant}} - n_a = -2 \cdot 10^{-3}$ and the loss $\alpha_{\mathrm{implant}} = 50\ \mathrm{cm}^{-1}$. This means that the increase of the loss is supplemented by a decrease of the index. In addition, the CS gets the property of a waveguide. This could be the reason for the narrowing of the near-field intensity of the implanted device [compare Figs. 7(b) and 6(b)] with a full width at half maximum (FWHM) of about 90 μm only. Because the absorption coefficient of the QW outside the CS region, and possibly of the other affected layers, rises too, the radiation taking the direct path to the facet is correspondingly absorbed.

The FWHM of the far-field intensity of the implanted device is 0.6° and is nearly power independent. The calculated far-field intensity is even narrower. It is worth noting that the exact shapes of the near- and far-field intensity profiles depend very sensitively on the parameters Δn_G and L.

The improvement in the shapes of the intensity profiles and their power independence finds its expression in the corresponding behavior of the times-diffraction-limit factor M^2 depicted in Fig. 8. M^2 was determined from the measured $1/\mathrm{e}^2$-intensity levels of the far- and near-field intensity profiles. Whereas for the nonimplanted device M^2 rises up to a value of three at the maximum output power measured (which is still one order of magnitude smaller than the M^2 value of an equivalent broad-area Fabry–Perot laser), M^2 remains nearly constant equal to 1.7 over the whole power range for the implanted device. Therefore, it can be hoped that by increasing the maximum output power of implanted devices, the M^2 factor can be kept below two.

The optical spectra of both devices depicted in Fig. 9 look very similar. They show only one longitudinal mode lasing with a side-mode suppression ratio (SMSR) of more than 28 dB and a spectral linewidth $\Delta\lambda$ (FWHM) of less than 6 pm. This confirms the high spectral selectivity of the α-DFB laser. The experimental values for the SMSR and for $\Delta\lambda$ are both limited by the optical spectrum analyzer used (spectral resolution 2 pm). The combination of small M^2, high output power, and small spectral linewidth yields a large spectral brightness, which is unique to the α-DFB laser [9].

V. Conclusion

The simulation of the α-DFB laser predicted a suppression of the side lobes in the near-field profile, and an improvement of beam quality, by an introduction of additional optical losses outside the CS. This prediction was confirmed experimentally by an ion implantation of the regions outside the CS. The linearity of the light–current characteristics has been extended from 1.3 W to 1.8 W output power. On the other hand, the maximum achievable output power decreased, too. The times-diffraction-limit factor M^2 of the implanted device remained constant equal to 1.7 over the whole power range. This gives reason to hope that by an optimization of device or implantation parameters, the output power can be increased again without loss of beam quality.

References

[1] S. O'Brien, R. J. Lang, R. Parke, J. Major, D. F. Welch, and D. Mehuys, "2.2 W continuous-wave diffraction-limited monolithically integrated master oscillator power amplifier at 854 nm," *IEEE Photon. Technol. Lett.*, vol. 9, pp. 440–442, Apr. 1997.

[2] B. Sumpf, G. Beister, G. Erbert, J. Fricke, A. Knauer, W. Pittroff, P. Ressel, J. Sebastian, H. Wenzel, and G. Tränkle, "2 W reliable operation of $\lambda = 735$ nm, GaAsP/AlGaAs laser diodes," *Electron. Lett.*, vol. 37, pp. 351–353, Mar. 2001.

[3] M. Kelemen, J. Weber, F. Rinner, J. Rogg, M. Mikulla, and G. Weimann, "High-brightness 1040 nm tapered diode lasers," in *Proc. SPIE*, vol. 4947, 2002, pp. 252–260.

[4] R. J. Lang, K. Dzurko, A. A. Hardy, S. DeMars, A. Schönfelder, and D. F. Welch, "Theory of grating-confined broad-area lasers," *IEEE J. Quantum Electron.*, vol. 34, pp. 2196–2210, Oct. 1998.

[5] K. M. Dzurko, R. J. Lang, D. F. Welch, D. R. Scifres, and A. Hardy, "650 mW cw single-mode operation of angled grating distributed feedback lasers," in *Proc. IEEE LEOS Conf.*, vol. 2, San Fransisco, CA, Nov. 1995, pp. 400–401.

[6] S. D. DeMars, A. Schönfelder, V. Wong, and R. J. Lang, "Optical properties of angled-grating distributed feedback lasers," in *Dig. IEEE Int. Semiconductor Laser Conf.*, Nara, Japan, Oct. 1998, pp. 57–58.

[7] V. V. Wong, S. D. DeMars, A. Schönfelder, and R. J. Lang, "Angled-grating distributed-feedback laser with 1.2 W cw single-mode diffraction-limited output at 1.06 μm," in *Proc. CLEO*, San Fransisco, CA, May 1998, pp. 34–35.

[8] K. Paschke, A. Bogatov, A. Drakin, R. Güther, A. Stratonnikov, H. Wenzel, G. Erbert, and G. Tränkle, "Modeling and measurements of the radiative characteristics of high-power α-DFB lasers," *IEEE J. Select. Topics Quantum Electron.*, vol. 9, pp. 835–843, May/June 2003.

[9] K. Paschke, F. Bugge, J. Fricke, R. Güther, G. Erbert, and G. Tränkle, "High power and high spectral brightness in 1060 nm α-DFB lasers with long resonators," *Electron. Lett.*, vol. 39, pp. 369–370, Feb. 2003.

[10] H. Kogelnik, "Coupled wave theory for thick hologram gratings," *Bell Syst. Tech. J.*, vol. 48, pp. 2909–2947, 1969.

[11] S. D. DeMars, R. J. Lang, and A. Schönfelder, "Angled Distributed Reflector Optical Device With Enhanced Light Confinement," U.S. Patent 6 122 299, Sept. 19, 2000.

[12] W. W. Bewley, I. Vurgaftman, R. E. Bartolo, M. J. Jurkovic, C. L. Felix, J. R. Meyer, H. Lee, R. U. Martinelli, G. W. Turner, and M. Manfra, "Limitations to beam quality of mid-IR angled-grating distributed feedback lasers," *IEEE J. Select. Topics Quantum Electron.*, vol. 7, pp. 96–101, Mar./Apr. 2001.

[13] R. Güther, "Beam propagation in an active planar waveguide with an angled Bragg grating (α-laser)," *J. Modern Opt.*, vol. 45, pp. 1537–1546, July 1998.

[14] G. C. Dente, "Modeling broad-area DBR/DFB lasers," in *Proc. SPIE*, vol. 2382, 1996, pp. 165–186.

[15] I. Vurgaftman, W. W. Bewley, R. E. Bartolo, C. L. Felix, M. J. Jurkovic, J. R. Meyer, M. J. Yang, H. Lee, and R. U. Martinelli, "Far field characterizations of mid-IR angled grating distributed feedback lasers," *J. Appl. Phys.*, vol. 88, pp. 6997–7005, Dec. 2000.

[16] J. Fricke, M. Matalla, K. Paschke, R. Güther, A. Knauer, F. Bugge, and H. Wenzel, "Fabrication and testing of Bragg gratings for 1060 nm α-DFB lasers," in *Proc. SPIE*, vol. 4947, 2002, pp. 223–231.

Katrin Paschke was born in Schwedt, Germany, in 1969. She received the Diploma degree in physics from University of Potsdam, Potsdam, Germany, in 1996. Since 1997, she has been with Ferdinand Braun Institut für Höchstfrequenztechnik, Berlin, Germany, where she is currently working toward the Ph.D. degree.

Her current research interests include modeling and design of the high-power α-DFB laser, as well as device fabrication and characterization.

Alexander Bogatov was born in Suchan, Russia, on September 15, 1947. He received the M.S. degree from Moscow Institute of Physics and Technology, Moscow, Russia, in 1971, and the candidate's and doctor's degrees in physics and mathematics from Lebedev Physical Institute (LPI), Moscow, Russia, in 1977 and 1996, respectively.

In 1971, he joined the Lebedev Physical Institute. Currently, he is the Head of the Injection Laser Laboratory of LPI and a Professor with the Moscow Institute of Physics and Technology. His current research interests are in semiconductor lasers, optics, waveguiding and optical nonlinearity, spectral and spatial distributions of optical fields, and intensity fluctuations in injection lasers, theoretical and experimental.

Dr. Bogatov was awarded the State Prize of the U.S.S.R. in physics in 1984.

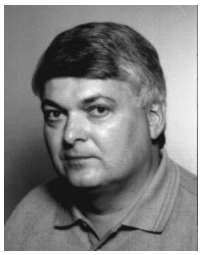

Frank Bugge received the Diploma and Ph.D. degrees from the Electrotechnical University, St. Petersburg, Russia, in 1975 and 1986, respectively.

Between 1975 and 1992, he was with the Werk fur Fernsehelektronik, Berlin, Germany, and was contributing to the development of optoelectronic devices and epitaxy of AIII-BV semiconductors. Since 1992, he has been with the Ferdinand Braun Institute, Berlin, Germany, and his work concentrates on MOVPE laser diodes in the emission wavelength range between 700 nm and 1200 nm. Since 1998, he has been responsible for the epitaxy development of laser diodes. His current research interests are focused on the development of high-power devices, increasing beam quality, and the effect of strain and strain compensation on the device.

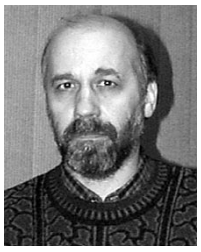

Alexander E. Drakin was born in Moscow, Russia, on March 23, 1954. He received the M.S. degree from the Moscow Institute of Physics and Technology, Moscow, Russia, in 1977, and the Candidate's degree in physics and mathematics from Lebedev Physical Institute (LPI), Moscow, Russia, in 1997.

In 1977, he joined the Optoelectronic Department of Lebedev Physical Institute, and is currently a Senior Researcher. Since joining LPI, he has been engaged in technology and research of the injection lasers on the base of InGaPA's and InGaAsSb solid solutions. Currently, his research interests include the design and investigation of laser diodes with high brightness.

Jörg Fricke received the diploma in physics from the University of Rostock, Rostock, Germany, in 1991. In 1996, he received the Doctor Engineer from the Technical University Berlin, Berlin, Germany.

His work was focused on the development of micromechanical accelerometers in silicon surface micromaching technology. From 1997–1998 he worked in the field of self-organized structures on GaAs at Paul-Drude Institute of Berlin, Germany, and in 1998, he joined the Ferdinand Braun Institut, Berlin, Germany, currently dealing with the fabrication of laser diodes.

Reiner Güther received the Diploma degree and the Dr. rer. nat. degree from the University of Jena, Jena, Germany, in 1964 and 1967, respectively, the Dr. sc. degree from the Academy of Sciences of Berlin, Germany, in 1976, the facultas docendi from the Technical University Ilmenau, Ilmenau, Germany, in 1982, and the Dr. habil. degree from University of Leipzig, Leipzig, Germany, in 1993.

From 1968 to 1991 he worked in the Central Institute of Optics and Spectroscopy (ZOS) Berlin of the Academy of Sciences, Berlin, Germany, in part as Department Head for Applied Optics. Since 1992, he has been a Researcher with the Ferdinand Braun Institut für Höchstfrequenztechnik, Berlin, Germany. His research activities include quantum field theory, nonlinear optics, volume holography, electro-optics, electromagnetic phenomena and correction theory of holographic concave gratings, diffractive optics, and waveguide coupling, mostly by direct order of the optics industry, such as Carl Zeiss or Telekom. His current research activities are the design of semiconductor lasers with planar filtering structures, and laser optics, including micro-optics.

Dr. Güther is a member of the Deutsche Gesellschaft für angewandte Optik (DGaO), the European Optical Society (EOS), and the IEEE Lasers and Electro-Optics Society (LEOS) (1995–2000).

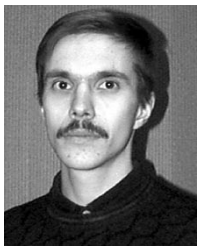

Alexey A. Stratonnikov was born in St. Petersburg, Russia, on December 4, 1977. He received the M.S. degree from the Moscow Institute of Physics and Technology, Moscow, Russia, in 1999, and is currently working toward the Candidate degree in physics and mathematics.

His research interests are in the simulation and research of semiconductor lasers.

Hans Wenzel received the Diploma and Doctoral degrees in physics from Humboldt University, Berlin, Germany, in 1986 and 1991, respectively.

From 1991 to 1994, he was involved in a research project on the three-dimensional simulation of DFB lasers. In 1994, he joined the Ferdinand Braun Institut für Höchstfrequenztechnik, Berlin, Germany, where he is engaged in the development of high-power semiconductor lasers, including DFB lasers.

Götz Erbert (M'95) received the Diploma degree in physics from Humboldt University, Berlin, Germany, in 1973, and the Doctoral degree in physics from the Academy of Sciences of the GDR, Berlin, Germany, in 1990.

From 1973 to 1991, he was with the Academy of Sciences, first on integrated optics dynamic holographic gratings in semiconductors, and later on semiconductor lasers. In 1992, he joined the Ferdinand Braun Institut, Berlin, Germany. Since 1996, he has been responsible for the optoelectronic activities in the Institute. He is working on high-power semiconductor lasers based on GaAs using strained-layer quantum-well active regions in the wavelength range from 650 to 1200 nm.

Günther Tränkle (M'95) received the Diploma degree in physics from the Technical University Munich, Munich, Germany, in 1981, and the Doctoral degree in physics from the University of Stuttgart, Stuttgart, Germany, in 1988, where he worked on quantization and many-body effects in III/V quantum well structures.

In 1988, he joined the Walter Schottky Institute, Technical University Munich, running its III/V-semiconductor technology and working on field-effect transistors and laser diodes. From 1995–1996, he was a Department Head with the Fraunhofer Institute for Applied Solid-State Physics, Freiburg, Germany, being responsible for the development and realization of electronic and optoelectronic III/V semiconductor devices, as well as quantum well infrared detector arrays. In August 1996, he became Head of the Ferdinand Braun Institute, Berlin, Germany. Since 2002, he has held a Chair on microwaves and optoelectronics at the Technical University Berlin, Berlin, Germany. His current research interests include III/V technology, micro- and mm-wave transistors and circuits, GaN electronics and high-power diode lasers.